# Synchrotron self-Compton flaring of TeV blazars: Combined linear and nonlinear electron cooling

Reinhard Schlickeiser
Institut für Theoretische Physik
Lehrstuhl IV: Weltraum- und Astrophysik
Ruhr-Universität Bochum, Germany

January 26, 2010

**Topics**:

1. Introduction
2. Nonlinearity of the SSC energy loss rate of electrons
3. Linear synchroton and nonlinear SST electron cooling
4. Combined linear synchrotron and nonlinear SST cooling
5. Intrinsic optically thin synchrotron radiation
6. Total synchrotron fluences
7. SEDs and light curves from numerical radiation code
8. Summary and conclusions

**References:**

Combined synchrotron and nonlinear synchrotron-self-Compton cooling of relativistic electrons, R. Schlickeiser, M. Böttcher and U. Menzler, 2010, Astron. Astrophys., submitted

Nonlinear synchrotron self-Compton cooling of relativistic electrons; R. Schlickeiser, 2009, MNRAS 398, 1483.

Synchrotron self-Compton flaring of TeV blazars I. Linear electron cooling; R. Schlickeiser and C. Röken, 2008, Astron. Astrophys. 477, 701

# 1. Introduction

The broadband SEDs of blazars exhibit two broad spectral components. In leptonic models the low-energy component is attributed to synchrotron radiation of relativistic electrons whereas the high-energy component results from synchroton-self Compton (SSC) interactions of the relativistic electrons, inverse Compton upscattering the synchrotron photons.

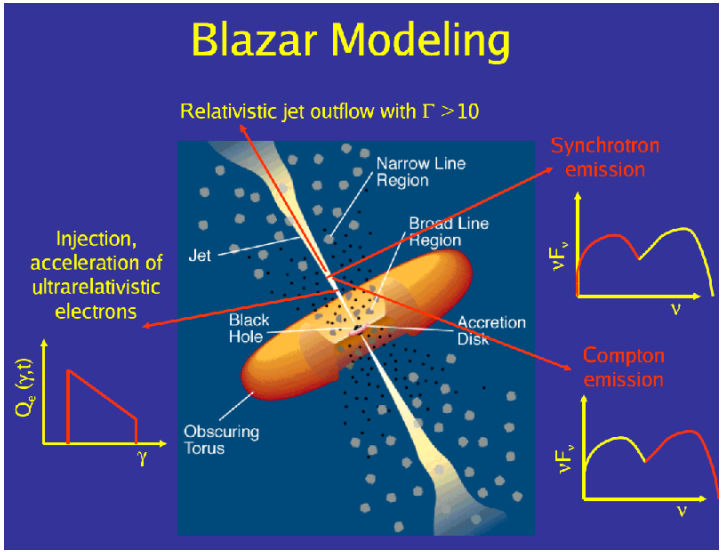

The Fermi survey of blazars (Abdo et al. 2009) and multiwavelength monitoring of the individual blazars PKS 0528+134 (Aharonian et al. 2005), 1ES 1121-232 (Aharonian et al. 2007b), PKS 0528+134 (Sambruna et al. 1997) and Mrk 421 (Fossati et al. 2008) have shown that during high state phases the SSC component dominates over the synchrotron component implying that the inverse Compton SSC losses of electrons are at least equal or greater than the synchrotron losses of electrons, even more when the intergalactic deabsorption of the TeV emission from the cosmic infrared background is factored in. The linear synchrotron cooling, included standardly in radiation models of blazars, then has to be replaced by the SSC cooling.

$$L_S = mc^2 \int dV \int_1^\infty d\gamma \; n(\gamma) |\dot{\gamma_S}|,$$
$$L_{SSC} = mc^2 \int dV \int_1^\infty d\gamma \; n(\gamma) |\dot{\gamma_{SSC}}| \qquad (1)$$

All physical quantities are calculated in a coordinate system comoving with the radiation source.

## 2. Nonlinearity of the SSC energy loss rate

For spatially isotropically distributed relativistic electrons the generated synchrotron photons also are spatially isotropically distributed with the differential number density

$$n_S(\epsilon, t) = \frac{4\pi R j_S(\epsilon, t)}{c\epsilon} \tag{2}$$

where $\epsilon$ denotes the synchrotron photon energy and $R$ is the radius of the spherical source. The spontaneous synchrotron emission coefficient

$$j_S(\epsilon, t) = \frac{1}{4\pi} \int_0^\infty d\gamma n(\gamma, t) p_s(\epsilon, \gamma) \tag{3}$$

is calculated from the electron distribution function and the synchrotron power of a single electron. The synchrotron power of a single electron (Crusius and Schlickeiser 1988) in a large-scale random magnetic field of constant strength $B$ is

$$p_s(\epsilon, \gamma) = \frac{P_0 \epsilon}{\gamma^2} CS\left(\frac{2\epsilon}{3\epsilon_0 \gamma^2}\right), \; CS(x) = W_{0,\frac{1}{3}}(x) W_{0,\frac{4}{3}}(x) - W_{\frac{1}{2},\frac{5}{6}}(x) W_{-\frac{1}{2},\frac{5}{6}}(x) \tag{4}$$

$\gamma$ is the electron Lorentz factor, $P_0 = \alpha_f / 2\sqrt{3}\hbar = 3.2 \cdot 10^{12}$ eV$^{-1}$s$^{-1}$, $\epsilon_0 = 1.16 \cdot 10^{-8} b$ eV for a magnetic field strength $B = b$ Gauss.

The SSC power of a single electron is (Schlickeiser 2002, Ch. 4.2) is

$$p_{\rm SSC}(\epsilon_s,\gamma) = c\int_0^\infty d\epsilon n_S(\epsilon,t)\epsilon_s\sigma(\epsilon_s,\epsilon,\gamma) \tag{5}$$

with the differential Klein-Nishina cross section (Blumenthal and Gould 1970)

$$\sigma(\epsilon_s,\epsilon,\gamma) = \frac{3\sigma_T}{4\epsilon\gamma^2}G(q,\Gamma) \tag{6}$$

with

$$G(q,\Gamma) = G_0(q) + \frac{\Gamma^2q^2(1-q)}{2(1+\Gamma q)},\ G_0(q) = 2q\ln q + (1+2q)(1-q), \tag{7}$$

and

$$\Gamma = \frac{4\epsilon\gamma}{mc^2},\ \ q = \frac{\epsilon_s}{\Gamma(\gamma mc^2-\epsilon_s)} \tag{8}$$

$\epsilon_s$ denotes the scattered photon energy, $\gamma$ is the electron Lorentz factor, $c$ denotes the speed of light and $\sigma_T = 6.65\cdot10^{-25}$ cm$^2$ is the Thomson cross section.

The SSC energy loss rate of electrons is

$$|\dot{\gamma}|_{\rm SSC} = \frac{1}{mc^2}\int_0^{\epsilon_{s,\max}} d\epsilon_s p_{\rm SSC}(\epsilon_s,\gamma) =$$

$$\frac{3c\sigma_T}{4mc^2\gamma^2}\int_0^{\infty} d\epsilon \epsilon^{-1} n_S(\epsilon,t)\int_0^{\epsilon_{s,\max}} d\epsilon_s \epsilon_s G(q,\Gamma) \qquad (9)$$

where $\epsilon_{s,\max} = \Gamma\gamma mc^2/(\Gamma+1)$ corresponds to $q=1$. Using $q$ as integration variable instead of $\epsilon_s$ results in

$$|\dot{\gamma}|_{\rm SSC} = \frac{12c\sigma_T}{mc^2}\gamma^2\int_0^{\infty} d\epsilon \epsilon n_S(\epsilon,t) J(\Gamma) \qquad (10)$$

with the integral $J(\Gamma) = \int_0^1 dq\, qG(q,\Gamma)(1+\Gamma q)^{-3}$ yielding

$$J(\Gamma \ll 1) \simeq \frac{1}{9}; \quad J(\Gamma \gg 1) \simeq \frac{1}{2\Gamma^2}\left[\ln\Gamma - \frac{11}{6}\right] \qquad (11)$$

In the Klein-Nishina range ($\Gamma \gg 1$) the inverse Compton losses are much reduced, as compared to the Thomson range ($\Gamma \ll 1$), and therefore negligible ($J(\Gamma > 1) = 0$). We find for the SSC energy loss rate in the Thomson limit – hereafter referred to as SST-cooling

$$|\dot{\gamma}|_{\rm SSC,TL} \simeq \frac{4c\sigma_T}{3mc^2}\gamma^2 W_s(t), \quad W_s(t) = \int_0^{\frac{mc^2}{4\gamma}} d\epsilon \epsilon n_S(\epsilon,t) \qquad (12)$$

Inserting Eqs. (2) – (4) we obtain

$$W_s(t) = \frac{4\pi R}{c}\int_0^{\frac{mc^2}{4\gamma}} d\epsilon j_S(\epsilon,t) = \frac{P_0 R}{c}\int_0^{\infty} dg\, g^{-2} n(g,t)\int_0^{\frac{mc^2}{4\gamma}} d\epsilon\, \epsilon CS\left(\frac{2\epsilon}{3\epsilon_0 g^2}\right) =$$

$$\frac{9P_0 R\epsilon_0^2}{4c}\int_0^{\infty} dg\, g^2 n(g,t)\int_0^{g_c^2/g^2} dx\, xCS(x) \qquad (13)$$

with

$$g_c(\gamma) = \sqrt{\frac{mc^2}{6\epsilon_0\gamma}} = \frac{2.21\cdot 10^4}{b^{1/2}\gamma^{1/2}} \qquad (14)$$

The dominant contribution to the double integral in Eq. (13) results from the interval $g < g_c$ yielding

$$W_s(t) \simeq \frac{9P_0 R\epsilon_0^2 c_1}{4c}\int_0^{g_c} dg\, g^2 n(g,t) \qquad (15)$$

where $c_1 = \int_0^{\infty} dx\, xCS(x) = \frac{32}{81}\sqrt{3} = 0.684$
We now require that the maximum(=initial) electron Lorentz factor is such that $\gamma_0 < g_C(\gamma_0)$ (better fulfilled for Fermi blazars) which is equivalent to

$$\gamma_0 < \left[\frac{mc^2}{6\epsilon_0}\right]^{1/3} = 1.7\cdot 10^4 b^{-1/3} \qquad (16)$$

In this case the effective energy density in synchrotron photons equals the total energy density in synchrotron photons

$$W_s(t) \simeq \frac{9P_0R\epsilon_0^2c_1}{4c}\int_0^\infty d\gamma\,\gamma^2 n(\gamma,t) \tag{17}$$

The SST energy loss rate (12) then becomes

$$|\dot{\gamma}|_{\rm SST} \simeq A_0\gamma^2\int_0^\infty d\gamma\,\gamma^2 n(\gamma,t),\quad A_0=\frac{3c_1\sigma_T P_0 R\epsilon_0^2}{mc^2} \tag{18}$$

which depends on the energy integral of the actual electron spectrum.

# 3. Linear synchroton and nonlinear SST electron cooling

The competition between the instantaneous injection of ultrarelativistic electrons ($\gamma_0 \gg 1$) at the rate $Q(\gamma,t) = q_0\delta(\gamma-\gamma_0)\delta(t)$ at time $t=0$ and the electron synchrotron energy losses is described by the time-dependent kinetic equation for the volume-averaged relativistic electron population inside the radiating source (Kardashev 1962):

$$\frac{\partial n(\gamma,t)}{\partial t} - \frac{\partial}{\partial\gamma}\left[|\dot\gamma| n(\gamma,t)\right] = q_0\delta(\gamma-\gamma_0)\delta(t) \qquad (19)$$

## 3.1. Linear synchrotron cooling

The energy loss rate of relativistic electrons due to synchrotron radiation in a large-scale random magnetic field of constant energy density $U_B = B^2/8\pi$ is

$$|\dot\gamma|_S = D_0\gamma^2, \quad D_0 = \frac{4}{3}\frac{c\sigma_T}{mc^2}U_B = 1.29\cdot 10^{-9} b^2 \ \ \mathrm{s}^{-1} \qquad (20)$$

The solution of this kinetic equation is ($H$ denotes Heaviside step function)

$$n_S(\gamma,\gamma_0,t) = q_0 H[\gamma_0-\gamma]\delta\left(\gamma-\gamma_S(t)\right), \quad \gamma_S(t) = \frac{\gamma_0}{1+D_0\gamma_0 t} \qquad (21)$$

The half-life time, $t_s$ is

$$t_s = \frac{1}{D_0 \gamma_0} = \frac{7.75 \cdot 10^4}{\gamma_4 b^2} \quad \text{s} \tag{22}$$

where we scale $\gamma_0 = 10^4 \gamma_4$.

## 3.2. SST cooling

The case of solely SST cooling is solved in Schlickeiser (2009) giving for the nonlinear SST-solution

$$n_{SST} = q_0 H[\gamma_0 - \gamma] \delta\left(\gamma - \gamma_{SST}(t)\right), \quad \gamma_{SST}(t) = \frac{\gamma_0}{\left[1 + 3A_0 q_0 \gamma_0^3 t\right]^{1/3}} \tag{23}$$

implying the modified SST energy loss rate $|\dot{\gamma_{SST}}| = A_0 q_0 \gamma_{SST}^4$. The half-life time, $t_{1/2}^{SST}$, is

$$t_{1/2}^{SST} = \frac{7}{3A_0 q_0 \gamma_0^3} = 9.02 q_5^{-1} b^{-2} R_{15}^{-1} \gamma_4^{-3} \quad \text{s} \tag{24}$$

with the scalings $R = 10^{15} R_{15}$ cm and $q_0 = 10^5 q_5$ electrons cm$^{-3}$.
In comparison to the linear synchrotron loss time (22) the SST loss time not only depends differently on the initial electron Lorentz factor but also depends on the initial kinetic energy of injected electrons (proportional to $q_0 \gamma_0$) and the source radius $R$ because these quantities determine the number density of

the target synchrotron photons. The more electrons are injected, the stronger the magnetic field and the more compact the source region, the quicker each electron cools under the SST process. **Such a collective behaviour is new and completely different from the linear case.**

# 4. Combined linear synchrotron and nonlinear SST cooling

(Schlickeiser, Böttcher, Menzler 2010)
For combined synchrotron and SST cooling (18) the kinetic equation of the electrons (25) reads with the substitution $y = A_0 t$

$$\frac{\partial n(\gamma,t)}{\partial y} - \frac{\partial}{\partial \gamma}\left[\gamma^2 n(\gamma,t)\left(K_0 + \int_0^\infty d\tilde{\gamma}\,\tilde{\gamma}^2 n(\tilde{\gamma},t)\right)\right] = q_0\delta(\gamma-\gamma_0)\delta(y) \quad (25)$$

where $K_0 = D_0/A_0$. We set $S = \gamma^2 n$ and use $x = 1/\gamma$ as independent variable to obtain

$$\frac{\partial S}{\partial y} + \frac{\partial S}{\partial x}\left[K_0 + \int_0^\infty d\tilde{x}\tilde{x}^{-2} S(\tilde{x},y)\right] = q_0\delta(x-x_0)\delta(y) \quad (26)$$

Now we define the implicit time variable $T$ through

$$\frac{dT}{dy} = U(y) = K_0 + \int_0^\infty dx x^{-2} S(x,y) \quad (27)$$

Then Eq. (26) becomes

$$\frac{\partial S}{\partial T} + \frac{\partial S}{\partial x} = q_0\delta(x-x_0)\delta(T) \quad (28)$$

which is solved by the method of characteristics (or double Laplace transform) as

$$S(x,T) = q_0\delta(x-T-x_0)\left(H[T]-H[T-x]\right) \tag{29}$$

The final step is then to calculate explicitely the time variable $T$ as a function of $y$. Use Eq. (29) in Eq. (27) to write

$$\frac{dT}{dy} = K_0 + \int_0^\infty dx x^{-2} S(x,y) =$$

$$K_0 + q_0 \int_0^\infty dx x^{-2}\delta(x-T-x_0)\left(H[T]-H[T-x]\right)$$

$$= K_0 + q_0 H[T]H[x_0]\frac{1}{(x_0+T)^2} = K_0 + \frac{q_0}{(x_0+T)^2} \tag{30}$$

for $x_0 > 0$ and $T \geq 0$. With $z(y) = x_0 + T(y)$, Eq. (30) becomes

$$\frac{dz}{dy} = K_0 + \frac{q_0}{z^2} = \frac{q_0 + K_0 z^2}{z^2}, \tag{31}$$

which after separation of variables with the integration constant $C_1$ leads to

$$K_0 y + C_1 = z - \int \frac{dz}{1+\frac{K_0 z^2}{q_0}} = z - \sqrt{\frac{q_0}{K_0}}\arctan\left(\sqrt{\frac{K_0}{q_0}}z\right), \tag{32}$$

or

$$x_0 + T(y) - \sqrt{\frac{q_0}{K_0}}\arctan\left(\sqrt{\frac{K_0}{q_0}}[x_0+T(y)]\right) = K_0 y + C_1 \tag{33}$$

The integration constant $C_1$ is fixed by the condition that $T = 0$ for $y = 0$ yielding

$$K_0 y = T - \sqrt{\frac{q_0}{K_0}}\left[\arctan\left(\sqrt{\frac{K_0}{q_0}}[x_0 + T(y)]\right) - \arctan\left(\sqrt{\frac{K_0}{q_0}}x_0\right)\right] \quad (34)$$

Unfortunately, for $K_0 \neq 0$ this dependence $y(T)$ cannot be inverted to infer the general dependence $T(y)$. However, an approximate inversion is possible by using the asymptotic expansions of the $\arctan$-function for small and large arguments compared to unity.

## 4.1. Injection parameter

The argument of the $\arctan$-function is always larger than $\alpha^{-1} = x_0(K_0/q_0)^{1/2}$. Therefore, we have to consider the two cases (i) $\alpha \geq 1$ and $\alpha < 1$, respectively. The parameter $\alpha$ depends on the energy density of the initially injected relativistic electrons and can be written as

$$\alpha = \frac{q_0^{1/2}}{K_0^{1/2}x_0} = \frac{q_0^{1/2}\gamma_0}{K_0^{1/2}} = \frac{\gamma_0}{\gamma_B} = 46\frac{\gamma_4 N_{50}^{1/2}}{R_{15}} \quad (35)$$

with the characteristic Lorentz factor

$$\gamma_B = \frac{K_0^{1/2}}{q_0^{1/2}} = \frac{2}{3}\sqrt{\frac{cU_B}{c_1 P_0 R\epsilon_0^2 q_0}} = \frac{217R_{15}}{N_{50}^{1/2}} \quad (36)$$

for standard blazar parameters $R = 10^{15} R_{15}$ cm and the total number of instantaneously injected electrons $N = 4\pi R^3 q_0/3 = 10^{50} N_{50}$, where we scale the electron injection Lorentz factor $\gamma_0 = 10^4 \gamma_4$.
Obviously, the more compact the source is, and the more electrons are injected, the smaller the characteristic Lorentz factor $\gamma_B$ is. If the injection Lorentz factor $\gamma_0$ is higher (smaller) than $\gamma_B$, the injection parameter $\alpha$ will be larger (smaller) than unity. For a compact sources with a large number of injected relativistic electrons the injection parameter $\alpha$ is much larger than unity.
For small values of the injection parameter $\alpha < 1$, corresponding to $\gamma_0 < \gamma_B$, the time evolution of the electron distribution function is solely determined by the linear synchrotron losses, whereas for large injection parameters $\alpha > 1$, corresponding to $\gamma_0 > \gamma_B$, nonlinear SST losses determine the electron distribution function at early times. Hence, the time evolution of the electron distribution function is affected by the nonlinear SST losses only if the injection Lorentz factor $\gamma_0$ exceeds the characteristic value $\gamma_B$ which is determined by the number of injected electrons and the size of the source.

## 4.2. Small injection energy $\gamma_0 < \gamma_B$

In the case of small injection energies $\gamma_0 < \gamma_B$ the injection parameter $\alpha < 1$ is smaller than unity, so that the argument of the $\arctan$-function in Eq. (33) is always larger than unity. For all values of $T$ and $y$ Eq. (33) then simplifies to

$$x_0 + T(y) \simeq K_0 y + C_0, \tag{37}$$

and with $C_0 = x_0$ to

$$T(y) \simeq K_0 y \tag{38}$$

In terms of $y$ the solution (30) then reads with $x_0 > 0$

$$S(x, x_0, y) = q_0 H[x - x_0]\delta\left(x - x_0 - K_0 y\right), \tag{39}$$

yielding

$$\begin{aligned} n(\gamma, \gamma_0, t) &= \frac{q_0}{\gamma^2} H[\gamma_0 - \gamma]\delta\left(\gamma^{-1} - \gamma_0^{-1} - D_0 t\right) \\ &= q_0 H[\gamma_0 - \gamma]\delta\left(\gamma - \frac{\gamma_0}{1 + D_0 \gamma_0 t}\right), \end{aligned} \tag{40}$$

which agrees with the standard linear synchrotron cooling solution (21).

### 4.3. High injection energy $\gamma_0 > \gamma_B$

In the case of high injection energies $\gamma_0 > \gamma_B$ the injection parameter $\alpha > 1$ is larger than unity. With the injection parameter (35) we rewrite Eq. (33) as

$$K_0 y + C_1 = \alpha x_0 \left[\frac{1 + \frac{T}{x_0}}{\alpha} - \arctan\left(\frac{1 + \frac{T}{x_0}}{\alpha}\right)\right] \tag{41}$$

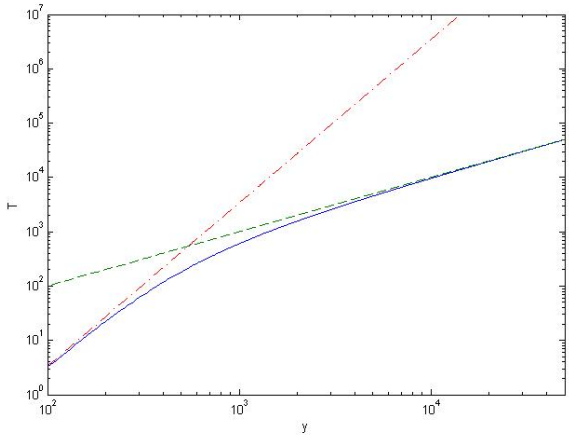


Figure 1: Comparison of exact solution $y(T)$ (full curve) with asymptotic solution $y_1(T)$ at small times (dashed curve) and asymptotic solution $y_2(T)$ at lates times (dotted curve) for the high injection energy case with $q_5 = 1$, $x_0 = 10^{-4}$ and $K_0 = 1$, corresponding to $\alpha = 3 \cdot 10^6$.

For small times $0 \leq T \leq T_c$, where

$$T_c = (\alpha - 1)x_0, \tag{42}$$

we use $\arctan(x) \simeq x - (x^3/3)$ to obtain

$$K_0 y_1 + C_1 \simeq \frac{x_0}{3\alpha^2}\left(1 + \frac{T}{x_0}\right)^3, \tag{43}$$

or

$$y_1 = \frac{(x_0 + T)^3}{3q_0} - C_2 \tag{44}$$

With $T = 0$ for $y = 0$ the integration constant $C_2 = x_0^3/3q_0$ is fixed so that

$$y_1 = \frac{(x_0 + T)^3}{3q_0} - \frac{x_0^3}{3q_0} \tag{45}$$

This solution is valid for $T \leq T_c$, corresponding with Eq. (42) to

$$0 \leq y \leq y_c = \frac{x_0^3}{3q_0}\left(\alpha^3 - 1\right) = \frac{x_0}{3\alpha^2 K_0}(\alpha^3 - 1) \tag{46}$$

For times $T \geq T_c$ or $y \geq y_c$ the argument of the $\arctan$-function in Eq. (41) is large compared to unity, yielding

$$K_0 y_2 + C_3 \simeq x_0 + T, \tag{47}$$

or the linear relation

$$y_2 = \frac{x_0 + T}{K_0} - C_4 \tag{48}$$

The constant $C_4$ is determined by the equality of the two solutions $y_1(T_c) = y_2(T_c) = y_c$ at $T_c$ providing

$$C_4 = \frac{\alpha x_0}{K_0} + \frac{x_0^3}{3q_0}(1-\alpha^3) = \frac{x_0^3}{3q_0}\left[1+2\alpha^3\right], \tag{49}$$

so that

$$y_2 = \frac{x_0 + T}{K_0} - \frac{2q_0^{1/2}}{3K_0^{3/2}} - \frac{x_0^3}{3q_0} \tag{50}$$

In Fig. 1 we compare the two approximate solutions (45) and (50) with the exact solution (34). The agreement is reasonably good.
Both approximate solutions (45) and (50) can be inverted to yield

$$T_1(y < y_c) = \left[3q_0 y + x_0^3\right]^{1/3} - x_0 = x_0\left[\left(1 + \frac{3\alpha^2 K_0 y}{x_0}\right)^{1/3} - 1\right] \tag{51}$$

and

$$T_2(y \geq y_c) = x_0\left[\frac{1}{3\alpha^2}\left(\frac{3\alpha^2 K_0 y}{x_0} + 1 + 2\alpha^3\right) - 1\right] \tag{52}$$

We then find for small times

$$n_1(\gamma,\gamma_0,t<t_c)=q_0H[\gamma_0-\gamma]H[t_c-t]\delta\left(\gamma-\frac{\gamma_0}{(1+3q_0\gamma_0^3A_0t)^{1/3}}\right), \quad (53)$$

which agrees with the nonlinear SST solution (23) of Schlickeiser (2009). At late times

$$n_2(\gamma,\gamma_0,t\geq t_c)=q_0H[\gamma_B-\gamma]H[t-t_c]\delta\left(\gamma-\frac{\gamma_B}{\frac{1+2\alpha^3}{3\alpha^3}+\gamma_BK_0A_0t}\right), \quad (54)$$

which is a modified linear cooling solution. Note that both solution show that at time

$$\begin{aligned} t_c &= \frac{y_c}{A_0}=\frac{\alpha^3-1}{3\alpha^3\gamma_BD_0}\simeq\frac{1}{3\gamma_BD_0} \\ &= \frac{2.6\cdot10^8}{\gamma_Bb^2}\,\mathrm{s}=\frac{1.2\cdot10^6N_{50}^{1/2}}{R_{15}b^2}\,\mathrm{s} \end{aligned} \quad (55)$$

the electrons have cooled to the characteristic Lorentz factor $\gamma_B$.

## 4.4. Interlude

Summarizing this section: provided electrons are injected with Lorentz factors higher than $\gamma_B$, given in Eq. (36), they initially cool down to the characteristic Lorentz factor $\gamma_B$ by nonlinear SST-cooling until time $t_c$ . At later times they further cool to lower energies according to the modified cooling solution (54). If the electrons are injected with Lorentz factors smaller than $\gamma_B$ they undergo only linear synchrotron cooling at all energies with no influence of the SST cooling. The characteristic Lorentz factor $\gamma_B$ is only determined by the injection conditions, whereas the time scale $t_c$ also depends on the magnetic field strength.

This different cooling behaviour for large and small injection energies affects the synchrotron and SSC intensities and fluences which we investigate in the next sections.

# 5. Intrinsic optically thin synchrotron radiation intensities

The optically thin synchrotron intensity $n(\gamma, t)$ is given by

$$I(\epsilon, t) = R j_S(\epsilon, t) = \frac{R}{4\pi} \int_0^\infty d\gamma \, n(\gamma, t) p_S(\epsilon, \gamma), \tag{56}$$

## 5.1. High injection energy

Inserting the electron density (53) gives at early times $t < t_c$

$$I_1(\epsilon, \tau < \tau_c) = \frac{3RP_0 q_0 \epsilon_0 \epsilon}{8\pi E_0} [1+\tau]^{2/3} \, CS\left(\frac{\epsilon[1+\tau]^{2/3}}{E_0}\right), \tag{57}$$

where we have introduced the initial characteristic synchrotron photon energy

$$E_0 = \frac{3}{2}\epsilon_0 \gamma_0^2 = 1.74 b \gamma_4^2 \quad \text{eV} \tag{58}$$

and the dimensionless time scale

$$\tau = 3A_0 q_0 \gamma_0^3 t = 3\alpha^2 D_0 \gamma_0 t = 3\alpha^2 t/t_s, \tag{59}$$

with the linear synchrotron cooling time $t_s = 7.75 \cdot 10^4 b^{-2} \gamma_4^{-1}$ s. Then

$$\tau_c = 3A_0 q_0 \gamma_0^3 t_c = \frac{q_0 \gamma_0^3}{\gamma_B K_0} \frac{\alpha^3 - 1}{\alpha^3} = \alpha^3 - 1, \tag{60}$$

Likewise, inserting the late electron density (54) gives

$$I_2(\epsilon, \tau \geq \tau_c) = \frac{RP_0 q_0 \epsilon_0 \epsilon}{24\pi\alpha^4 E_0} \left(1 + 2\alpha^3 + \tau\right)^2 CS\left(\frac{\epsilon}{9\alpha^4 E_0}\left[1 + 2\alpha^3 + \tau\right]^2\right) \tag{61}$$

in terms of the same dimensionless time (58).
The function $CS(x)$ is well approximated by (Crusius and Schlickeiser 1988)

$$CS(x) = a_0 x^{-2/3} e^{-x} \tag{62}$$

with $a_0 = 1.151275$ yielding

$$I_1(\epsilon, \tau < \tau_c) = \frac{3a_0}{8\pi} RP_0 q_0 \epsilon_0 (\epsilon/E_0)^{1/3} \left[1 + \tau\right]^{2/9} \exp\left(-\frac{\epsilon}{E_0}\left[1 + \tau\right]^{2/3}\right) \tag{63}$$

and

$$I_2(\epsilon, \tau \geq \tau_c) = \frac{3^{1/3} a_0 RP_0 q_0 \epsilon_0}{8\pi\alpha^{4/3}} (\epsilon/E_0)^{1/3} \left[1 + 2\alpha^3 + \tau\right]^{2/3} \exp\left(-\frac{\epsilon}{\epsilon_2}\right), \tag{64}$$

respectively, with the cut-off energies

$$\epsilon_1(\tau \leq \tau_c) = E_0(1 + \tau)^{-2/3},\ \epsilon_2(\tau \geq \tau_c) = 9\alpha^4 E_0 \left[1 + 2\alpha^3 + \tau\right]^{-2} \tag{65}$$

With respect to photon energy $\epsilon$ both synchrotron intensities exhibit the same increasing power law with exponential cut-off behaviour; however, the cut-off energy differs for small and late times due to the different electron cooling behaviour. Note that $\epsilon_1(\tau_c) = \epsilon_2(\tau_c) = E_0/\alpha^2$.
The cut-off energies (65) determine the time-dependence of the peak energy $\epsilon_p(\tau)$ of the synchrotron SED $\epsilon I(\epsilon, \tau)$. At early and late times times we obtain

$$\epsilon_p(\tau < \tau_c) = \frac{4\epsilon_1}{3} = \frac{4E_0}{3(1+\tau)^{2/3}} = \frac{4E_0}{3(1+3\alpha^2\frac{t}{t_s})^{2/3}} \tag{66}$$

and

$$\epsilon_p(\tau \geq \tau_c) = \frac{4\epsilon_1}{3} = \frac{12\alpha^4 E_0}{[1+2\alpha^3+\tau]^2} = \frac{12\alpha^4 E_0}{[1+2\alpha^3+3\alpha^2\frac{t}{t_s})]^2} \tag{67}$$

respectively, which is illustrated in Fig. 2.
For the high injection case the synchrotron peak energy decreases from its intial maximum value $E_{p,max} = (4E_0/3)$ proportional to $(1+\tau)^{-2/3}$ for small times $\tau < \tau_c = \alpha^3 - 1$ to $E_p = E_{p,max}/\alpha^2$. At later times $\tau \geq \tau_c$ the peak energy decreases further proportional to $\tau^{-2}$.

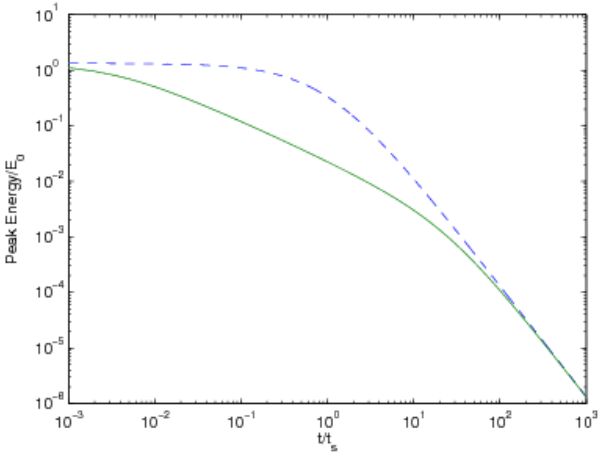


Figure 2: Time-dependence of the peak energy $\epsilon_p(t)$ of the synchrotron SED for high ($\alpha = 10$, lower curve) and low ($\alpha = 0.1$, upper curve) values of the injection parameter.

## 5.2. Small injection energy

For the small injection energy case $\alpha \ll 1$ we use the electron density (40) which in terms of the normalized time scale (58) reads

$$n(\gamma, \gamma_0, \tau) = q_0 H[\gamma_0 - \gamma]\delta\left(\gamma - \frac{\gamma_0}{1 + \frac{\tau}{3\alpha^2}}\right) \tag{68}$$

We obtain for the synchrotron intensity at all times

$$I(\epsilon, \tau) = \frac{3RP_0 q_0 \epsilon_0 \epsilon}{8\pi E_0}\left(1 + \frac{\tau}{3\alpha^2}\right)^2 CS\left(\frac{\epsilon}{E_0}\left[1 + \frac{\tau}{3\alpha^2}\right]^2\right) \simeq$$

$$\frac{3a_0 RP_0 q_0 \epsilon_0}{8\pi}\left(\frac{\epsilon}{E_0}\right)^{1/3}\left(1 + \frac{\tau}{3\alpha^2}\right)^{2/3} \exp\left(-\frac{\epsilon}{E_0}[1 + \frac{\tau}{3\alpha^2}]^2\right) \tag{69}$$

Here the synchrotron peak energy

$$\epsilon_p = \frac{4E_0}{3(1 + \frac{\tau}{3\alpha^2})^2} = \frac{4E_0}{3(1 + \frac{t}{t_s})^2} \tag{70}$$

decreases from its intial maximum value $(4E_0/3)$ proportional to $t^{-2}$ for $t > t_s$. The upper curve in Fig. 2 refers to this case. Note that for large times the high and small injection energy cases yield the same $\propto t^{-2}$-decrease of the peak energy.

## 5.3. Light curve peak times

Eqs. (66), (67) and (70) also provide the photon energy dependences of the intrinsic light curve peak time or the time of maximum intensity of the synchrotron flare $t_{\max}(\epsilon) = t_s \tau_{\max}(\epsilon)/3\alpha^2$.
For the small injection energy case ($\alpha \ll 1$) we reproduce the well known relation

$$t_{\max}(\epsilon, \alpha \ll 1) = t_s \left( \frac{E_0}{3\epsilon} \right)^{1/2} - 1 \tag{71}$$

for all energies below $3E_0$.
For the high injection energy case ($\alpha \gg 1$) we obtain

$$t_{\max}(\epsilon, \alpha \gg 1) = t_s \begin{cases} \left(\frac{E_0}{3\epsilon}\right)^{1/2} - \frac{2\alpha^3+1}{3\alpha^3} & \text{for } \epsilon \leq \frac{E_0}{3\alpha^2}, \\ \frac{1}{3\alpha^2}\left[\left(\frac{E_0}{3\epsilon}\right)^{3/2} - 1\right] & \text{for } \epsilon \geq \frac{E_0}{3\alpha^2}. \end{cases} , \tag{72}$$

indicating a steeper power law ($t_{\max} \propto \epsilon^{-3/2}$) at photon energies above $E_0/3\alpha^2$, whereas at lower energies the standard ($\propto \epsilon^{-1/2}$) dependence results.
This is also clearly visible in Fig. 3 where we compare the light curve peak times for small and high injection energy conditions. Note that at large photon energies $\epsilon > E_0/3\alpha^2$ the high injection peak time is a factor $3\alpha^2$ shorter than the small injection peak time. This results from the faster additional SST cooling of relativistic electrons in the high injection case.

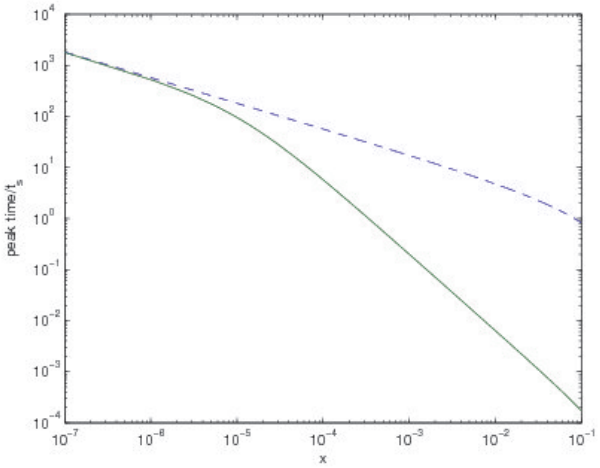


Figure 3: Photon energy ($x = \epsilon/E_0$) dependence of the synchrotron light curve peak time for high ($\alpha = 100$, full curve) and low ($\alpha = 0.1$, dashed curve) values of the injection parameter.

# 6. Total synchrotron fluences

In order to collect enough photons, intensities are often averaged or integrated over long enough time intervals. For rapidly varying photon intensities this corresponds to fractional fluences which are given by the time-integrated intensities $F_f(\epsilon, t_f) = \int_0^{t_f} dt\, I(\epsilon, t)$. The total fluence spectra result in the limit $t_f \to \infty$

$$F(\epsilon) = F_f(\epsilon, t_f = \infty) = \int_0^\infty dt\, I(\epsilon, t) = \frac{1}{3A_0 q_0 \gamma_0^3} \int_0^\infty d\tau\, I(\epsilon, \tau) \qquad (73)$$

## 6.1. Small injection energy

The synchrotron intensity (69) yields for the total fluence

$$F_s(\epsilon) = F_{0S} \left(\frac{E_0}{\epsilon}\right)^{1/2} \int_{\epsilon/E_0}^\infty dx\, x^{1/2} CS\,(x)\,, \qquad (74)$$

(with the constant $F_{0S} = 3\alpha^2 R P_0 \epsilon_0/(16\pi A_0 \gamma_0^3)$) with the asymptotics

$$F_s(\epsilon) \simeq F_{0S} \begin{cases} c_0 \left(\frac{E_0}{\epsilon}\right)^{1/2} & \text{for } \epsilon \ll E_0, \\ \left(\frac{E_0}{\epsilon}\right) \exp\left(-\epsilon/E_0\right) & \text{for } \epsilon \gg E_0. \end{cases} \qquad (75)$$

## 6.2. High injection energy

Here the synchrotron intensities (57) and (61) yield after obvious substitutions for the total synchrotron fluence

$$F_h(\epsilon) = \frac{1}{3A_0 q_0 \gamma_0^3}\left[\int_0^{\tau_c} d\tau\, I_1(\epsilon,\tau) + \int_{\tau_c}^{\infty} d\tau\, I_2(\epsilon,\tau)\right]$$

$$= F_{0h}\left(\frac{E_0}{\epsilon}\right)^{3/2}\left[\int_{\epsilon/E_0}^{\epsilon\alpha^2/E_0} dx\, x^{3/2} CS\,(x) + \frac{\epsilon\alpha^2}{E_0}\int_{\epsilon\alpha^2/E_0}^{\infty} dx\, x^{1/2} CS\,(x)\right] \quad (76)$$

(with the constant $F_{0h} = \frac{3RP_0\epsilon_0}{16\pi A_0\gamma_0^3}$) and the asymptotics

$$F_h(\epsilon) \simeq F_{0h}\begin{cases} c_0\alpha^2\left(\frac{E_0}{\epsilon}\right)^{1/2} & \text{for } \epsilon \ll E_0/\alpha^2, \\ c_2\left(\frac{E_0}{\epsilon}\right)^{3/2} & \text{for } E_0/\alpha^2 \ll \epsilon \ll E_0, \\ \left(\frac{E_0}{\epsilon}\right)\exp\left(-\epsilon/E_0\right) & \text{for } \epsilon \gg E_0. \end{cases} \quad (77)$$

At high synchrotron photon energies ($\epsilon \gg E_0$) the total synchrotron fluences for small and high injection energy exhibit the same exponential cut-off.
However, at low energies ($\epsilon \ll E_0$): in the small injection energy case the total synchrotron fluence exhibits the single power law behaviour $\propto \epsilon^{-1/2}$. In the high injection energy case the total synchrotron fluence steepens from the power law $\propto \epsilon^{-1/2}$ below $E_0/\alpha^2$ to the power law $\propto \epsilon^{-3/2}$ above $E_0/\alpha^2$.

## 6.3. Total fluence synchrotron SED

For the total fluence SED $S(\epsilon) = \epsilon F(\epsilon)$ we then find in the two cases of small (s) and high (h) inhection energies

$$S_s(\epsilon) = S_0 \frac{\alpha^2}{\gamma_0} \left( \frac{\epsilon}{E_0} \right)^{1/2} \exp\left(-\epsilon/E_0\right) \tag{78}$$

and

$$S_h(\epsilon) = S_0 \frac{\alpha^2}{\gamma_0} \left( \frac{\epsilon}{E_0} \right)^{1/2} \frac{\epsilon_B}{\epsilon + \epsilon_B} \exp\left(-\epsilon/E_0\right), \tag{79}$$

with the constant $S_0 = 3c_0 mc^2/32c_1\sigma_T$ and the characteristic break energy

$$\epsilon_B = \frac{c_2 E_0}{c_0 \alpha^2} = 0.703 \frac{E_0}{\alpha^2} \tag{80}$$

Fig. 4 shows the fluence SEDs $N(x)$, $x = \epsilon/E_0$, for small ($\alpha_s = 0.1$) and high ($\alpha_h = 100$) injection conditions.
The ratio of peak values is given by

$$\mathcal{R} = \frac{N_{h,peak}}{N_{s,peak}} \simeq 0.97 \frac{\alpha_h}{\alpha_s^2} \tag{81}$$

For the case shown in Fig. 4 this ratio is $\mathcal{R} = 9.7 \cdot 10^3$.

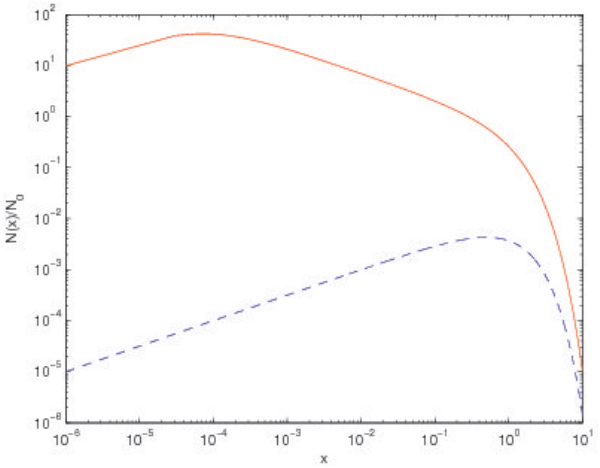


Figure 4: Total synchrotron fluence SED $N(x)$ as a function of $x = \epsilon/E_0$ for high ($\alpha_h = 100$, full curve) and small ($\alpha_s = 0.1$, dashed curve) injection conditions calculated for $\gamma_0 = 10^4$.

## 6.4. Summary of the differences

D1) In the high injection case the synchrotron SED peaks at a photon energy which is a factor $2x_B = 1.4\alpha_h^2 = 1.4 \cdot 10^{-4}$ smaller than the peak in the small injection case.
D2) The high injection energy peak value decreases at small times $t < \alpha t_s/3$ more rapidly than the small injection energy peak value.
D3) The high injection SED is a broken power law with spectral indices $+0.5$ below and $-0.5$ above the peak energy $x_B \ll 1$, respectively, and it cuts-off exponentially at photon energies $x > 1$. Below the peak energy $x_B$ the time of maximum synchrotron intensity decreases as $t_{\max} \propto \epsilon^{-1/2}$, whereas above the peak energy $x_B$ it decreases more rapidly as $t_{\max} \propto \epsilon^{-1/2}$ due to the severe additional SST losses.
D4) The small injection SED is a single power law with spectral indices $+0.5$ below the peak energy $0.5$, and it cuts-off exponentially at photon energies $x > 1$. Here the time of maximum synchrotron intensity decreases as $t_{\max} \propto \epsilon^{-1/2}$ at all energies $x < 1$ because in the small injection case the SST-losses do not contribute.
All four features are quantitatively visible in Figs. 2-4. These predicted differences for the total synchrotron fluence SED and the synchrotron light curve behaviours provides a conclusive test for the presence of high or low injection energy conditions in blazars.

# 7. Synchrotron and SSC fluence SEDs and light curves from numerical radiation code

In Fig. 5 we show the photon energy variation of the light curve peak time calculated with the numerical radiation code of Böttcher et al. (1997) using a magnetic field strength $b = 1$ and an injection Lorentz factor $\gamma_0 = 10^4$ for the high ($\alpha_h = 100$) and small ($\alpha_s = 0.1$) injection case. The numerical variations are in perfect agreement with the different power-law variations found analytically, which are included in Fig. 5 for orientation, and confirm our earlier findings.

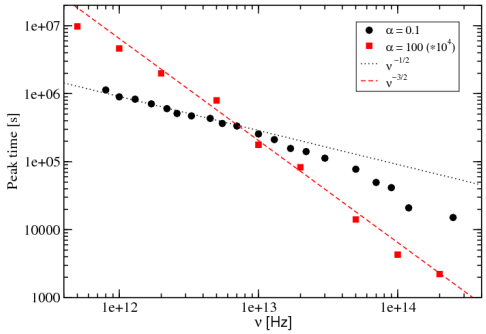


Figure 5: Numerically calculated synchrotron light curve peak times for small ($\alpha_s = 0.1$) and high ($\alpha_h = 100$) injection conditions calculated for $\gamma_0 = 10^4$ and $b = 1$.

In Fig. 6 and 7 we show the numerical synchrotron and SSC SEDs using a magnetic field strength $b = 1$ and an injection Lorentz factor $\gamma_0 = 10^4$ for the high ($\alpha_h = 100$) and small ($\alpha_s = 0.1$) injection case.
Both synchrotron SEDs are in remarkable agreement with the analytical SEDs shown in Fig. 4. In particular, the numerical SEDs confirm all four predicted differences listed in the last section. For orientation, we have plotted in both figures the asymptotic analytical synchrotron spectra as dashed and dash-dotted lines.

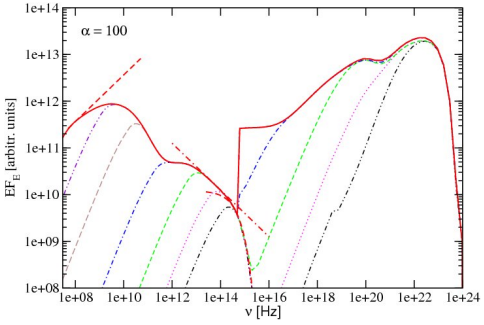


Figure 6: Numerically calculated fractional and total synchrotron and SSC fluence SEDs for high ($\alpha_h = 100$) injection conditions calculated for $\gamma_0 = 10^4$. Note that the SSC emission has been artificially cut off at low frequencies as it would otherwise overwhelm the high-energy end of the synchrotron emission.

The radiation code also yields the SSC fluence SEDs. We note from Figs. 6 and 7 that for the high injection case the SSC SED has a much higher amplitude than the synchrotron SED, whereas the opposite holds for the low injection case. Moreover, both SSC SEDs peak at the same photon energy, although the SSC peak value in the high injection case is a factor $2 \cdot 10^7$ larger than in the small injection case.

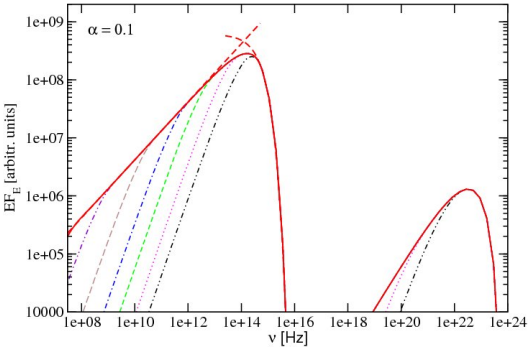


Figure 7: Numerically calculated fractional and total synchrotron and SSC fluence SEDs for small ($\alpha_s = 0.1$) injection conditions calculated for $\gamma_0 = 10^4$. The full curves show the total fluence SEDs. The dashed lines show the analytical asymptotes.

# 8. Summary and conclusions

- The broadband SEDs of blazars exhibit two broad spectral components which in leptonic emission models are attributed to synchrotron radiation and SSC radiation of relativistic electrons. If the high-frequency SSC component dominates over the low-frequency synchrotron component, the inverse Compton SSC losses of electrons are at least equal or greater than the synchrotron losses of electrons. The linear synchrotron cooling, included standardly in radiation models of blazars, then has to be replaced by the SSC cooling.

- The SSC energy loss rate of electrons calculated in the Thomson limit (SST cooling) exhibits nonlinear behaviour because it depends on an energy integral of the actual electron spectrum, reflecting the dependence of the energy density of the target synchrotron photons on the differential electron energy spectrum. The dependence on the initial kinetic energy of injected electrons is a collective effect completely different from the linear synchrotron case.

- For the illustrative case of instantaneous injection of monoenergetic particles we solve the nonlinear kinetic equation for the intrinsic temporal evolution of the relativistic particles under combined linear synchrotron and nonlinear SST-cooling.

- Qualitatively differenres for the light curves and SEDs resulting depending on whether electron cooling is initially Compton dominated (high injection energy parameter $\alpha$) or it is always synchrotron dominated (low $\alpha$). The injection parameter parameter $\alpha = \gamma_0/\gamma_B$ depends on the Lorentz factor $\gamma_0$ of injected electrons energy density of the initially injected relativistic electrons and can be written as and the characteristic Lorentz factor $\gamma_B = 217 R_{15} N_{50}^{-1/2}$, fixed by the source radius $R = 10^{15} R_{15}$ cm and the total number of instantaneously injected electrons $N = 10^{50} N_{50}$.

- In the low-$\alpha$ case, the resulting fluence spectrum exhibits a simple exponentially cut-off power-law behaviour, $S_\nu \propto \nu^{1/2} e^{-\nu/\nu_0}$. In contrast, in the high-$\alpha$ case, we find a broken power-law with exponential cutoff, parametrized in the form $S_\nu \propto \nu^{1/2} \frac{\nu_B}{\nu+\nu_B} e^{-\nu/\nu_0}$. Based on our analysis we propose the following interpretation of multiwavelength blazar SEDs:

- Blazars, where the $\gamma$-ray fluence is much larger than the synchrotron fluence, are regarded as high injection energy sources. Here, the synchrotron fluence should exhibit the symmetric broken power law behaviour around the synchrotron peak energy that is a factor $(\alpha_h \gamma_0)^2$ smaller than the SSC peak energy. Below and above $\nu_B$ the synchrotron light curve peak times exhibit different frequency dependences $t_{\max}(\nu < \nu_B) \propto \nu^{-1/2}$ and $t_{\max}(\nu > \nu_b) \propto \nu^{-3/2}$, respectively, resulting from the additional severe SST-losses at $\nu > \nu_B$.

- Blazars, where the $\gamma$-ray fluence is much smaller than the synchrotron fluence, are regarded as small injection energy sources. Here, the synchrotron fluence exhibits the single power law behaviour (D4) up to a higher synchrotron peak energy that is a factor $\gamma_0^2$ smaller than the SSC peak energy. In this case the synchrotron light curve peak time exhibits the standard linear synchrotron cooling decrease $t_{\max}(\nu) \propto \nu^{-1/2}$ at all frequencies.

- If the injection Lorentz factor $\gamma_0$ and the size of the source are the same, different values of the injection parameter $\alpha$ result from different total numbers of instantaneously injected electrons. E.g., the high injection case $\alpha_h = 100$ results for $N_{50} = 4.7$, whereas the low injection case $\alpha_s = 0.1$ needs $N_{50} = 4.7 \cdot 10^{-6}$.

- These predictions of spectral behaviour with time and frequency provide conclusive tests for the presence or absence of linear synchrotron cooling or nonlinear SST cooling in flaring nonthermal sources.

# Thanks to


- Ulf Menzler (Ruhr-Universität Bochum)
- Markus Böttcher (Ohio University)
- Christian Röken (Universität Potsdam)
- Ian Lerche (University of Halle)
- The HESS-Team
- Deutsche Forschungsgemeinschaft (Schl 201/20-1)


bmb+f - Förderschwerpunkt

Astroteilchenphysik

Großgeräte der physikalischen Grundlagenforschung